Network Formation of Tissue Cells via Preferential Attraction to Elongated Structures

Andras Szabo,[1] Erica D. Perryn,[2] and Andras Czirok[1,2]
[1]*Department of Biological Physics, Eotvos University, Budapest, Hungary*
[2]*Department of Anatomy and Cell Biology, KU Medical Center, Kansas City, Kansas, USA*
(Received 20 July 2006; published 18 January 2007)

Vascular and nonvascular cells often form an interconnected network in vitro, similar to the early vascular bed of warm-blooded embryos. Our time-lapse recordings show that the network forms by extending sprouts, i.e., multicellular linear segments. To explain the emergence of such structures, we propose a simple model of preferential attraction to stretched cells. Numerical simulations reveal that the model evolves into a quasistationary pattern containing linear segments, which interconnect above the critical volume fraction of 0.2. In the quasistationary state, the generation of new branches offset the coarsening driven by surface tension. In agreement with empirical data, the characteristic size of the resulting polygonal pattern is density-independent within a wide range of volume fractions.

DOI: 10.1103/PhysRevLett.98.038102 PACS numbers: 87.18.Ed, 87.17.Jj, 87.18.Bb, 87.18.Hf

Embryogenesis, the shaping of tissues and organs, is a long-standing challenge of science. Recent application of ideas originating from nonequilibrium statistical physics has proved to be fruitful for understanding emergent properties such as pattern formation or biomolecular network function during embryo development [1]. Formation of the primordial vascular bed of warm-blooded vertebrates is arguably one of the best examples for an emergent phenomenon in embryonic development [2]. During vasculogenesis, well before the onset of circulation, hundreds of essentially identical vascular endothelial cells create a polygonal network within a simple, sheetlike anatomical environment [Figs. 1(a) and 1(b)]. The network is highly variable among individuals within certain statistical constraints [3], relatively uniform in morphology, and, unlike insect segmentation, there is no evidence for direct genetic control of vascular segment positions.

The formation of linear segments and their interconnected network is not restricted to vascular endothelial cells [4]. In particular, we demonstrate in Figs. 1(c) and 1(d) that nonvascular, glia-related, or muscle-related cells also exhibit linear structures when grown on a rigid plastic tissue culture substrate with a continuously shaken culture medium. Depending on the cell density, the linear segments can merge and form an irregular network.

Recent *in vivo* observations of vasculogenesis indicated that early vascular network formation includes *sprouting*, the extension of linear segments containing multiple cells [5]. This process is markedly different from the gradual coarsening of an initially uniform density field, and its possible arrest, characteristic for colloid gels (see, e.g., [6]). To determine the mechanism of sprout formation, we recorded the temporal development of the structures shown in Figs. 1(b)–1(d) with computer controlled microscopy [7]. In vitro culture conditions yield sufficiently high resolution to trace the motion of individual cells during the patterning process. As shown in Figs. 1(e) and 1(f), sprout expansion involves cell motility guided by adjacent projections of other cells or elongated multicellular structures.

A number of theoretical models were formulated to understand the self-organization of vascular networks. The *chemomechanical* mechanism assumed cells to exert mechanical stress on the underlying substrate and the resulting stress to guide cell motility [8,9]. A recent model of Serini *et al.* and Gamba *et al.* assumed *chemoattractant* signaling [10,11]. While the suggested chemoattractant $VEGF_{165}$ is unlikely to behave in the predicted way (see the discussion in Ref. [12]), patterning guided by an unspecified chemoattractant continues to serve as the basis of biologically plausible models including cell adhesiveness and finite cell size [12].

Both the chemomechanical and chemoattractant mechanisms may be biologically relevant under certain circumstances. We argue, however, that neither can explain the sprout formation seen in Fig. 1. In both models, the patterns were reported to arise in a gradual coarsening process in which segments are eliminated and small holes are replaced with larger ones. Moreover, neither mechanism is expected to operate within our in vitro experimental setup: The rigid substrate excludes the chemomechanical mechanism. A specific chemotactic response is unlikely to be shared by such a variety of cell types. Finally, convection currents in the culture medium, generated by temperature inhomogeneities within the incubator and the vibrations of microscope stage motion, are expected to hamper the maintenance of concentration gradients or impose a strong directional bias upon the chemotaxis-related cell movements.

To measure the convection currents close to the culture surface, we immersed 0.5 μm diameter latex beads (Sigma) into the medium. Bead motion was recorded within a 20 μm thick volume above the culture surface, delimited by the field depth of the 10× microscope objective. As a representative sample [Fig. 1(d), inset] demonstrates, in our experimental setup convection currents were

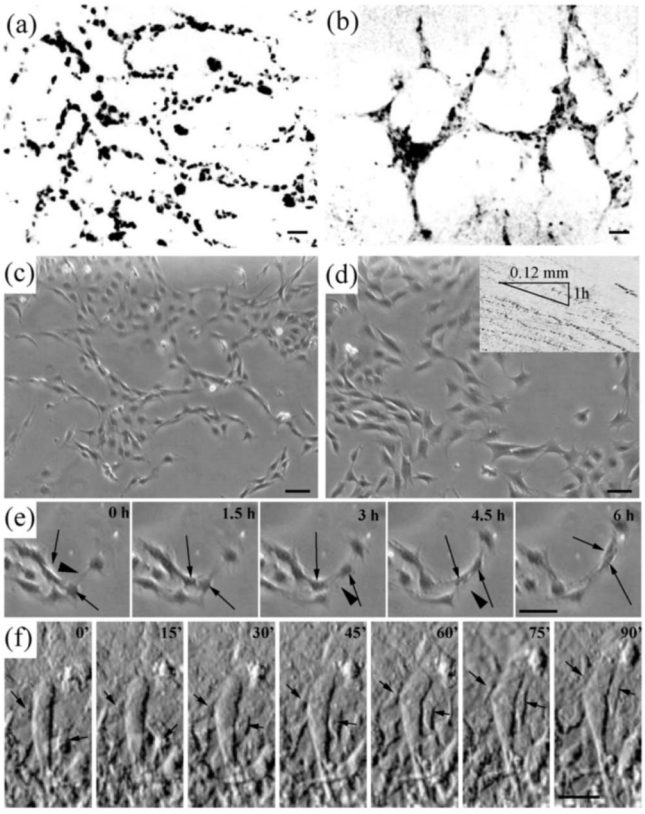

FIG. 1. Tissue cell networks. (a) Vascular endothelial cells during vasculogenesis, visualized in a bird embryo according to Ref. [7]. (b) Mouse vascular endothelial cells within an in vitro explant [22], after 24 h of culturing. (c) Astroglia-related rat C6 cells and (d) muscle-related mouse C2C12 cells cultured on a rigid tissue culture substrate as described in Ref. [23]. The inset depicts the motion of latex beads at the tissue culture surface. To measure convection currents, 10 μm wide and 250 μm long rectangles were selected in the images, directed parallel to the flow. For each frame, pixel intensities were averaged across the rectangle, resulting in the horizontal lines in the inset. (e) C6 cells (arrows) migrate along extended projections of adjacent cells (arrowheads). (f) Endothelial cells (arrows) move along a vascular sprout, visualized in the mouse explant by differential interference contrast microscopy.

sustained for hours with speeds exceeding 100 μm/h, an order of magnitude larger than the median cell speed.

On the basis of our empirical observations, in this Letter we propose that cellular sprouting employs a quite generic mechanism, the *preferential attraction to elongated structures*. While the molecular basis of such a behavior is unknown, one may conjecture two biologically feasible scenarios. (i) The tendency of cells to align with one another was analyzed in detail in myxobacteria (see, e.g., [13]), and similar mechanisms may also operate in animal cells. (ii) Cells in elongated structures are assumed to be under mechanical tension, and strained cells can have a stiffer cytoskeleton [14]. Cells are able to respond to variations in extracellular matrix stiffness [15], and an analogous mechanotaxis utilizing cell-cell contacts is also feasible. To assess the collective behavior of cells exhibiting the proposed preferential attraction property, we studied the following simple model in which individual cells are represented as particles.

Cell motility is often approximated as a persistent diffusion process [16,17], where the velocity $\vec{v}_k$ of cell k is described by the Langevin equation

$$\frac{d\vec{v}_k}{dt} = -\vec{v}_k/\tau + \sqrt{D}\vec{\xi}_k + \vec{M}_k, \tag{1}$$

where τ is the persistence time of motion, D is a diffusion parameter, and ξ is an uncorrelated white noise: $\langle\xi\rangle = 0$ and $\langle\xi_k(t)\xi_l(t')\rangle = \delta_{kl}\delta(t - t')$. Term $\vec{M}$ is a deterministic bias, representing interaction with the environment (specified below). While Eq. (1) describes the motion of a Brownian particle at finite temperatures, animal cell motility is driven by complicated molecular machinery, and it is *not* thermal fluctuation driven. Thus, parameters τ and D depend substantially on cell type and molecular state. Measurements performed with noninteracting endothelial cells and fibroblasts resulted τ and D values in the 0.1–5 h and 100–2000 $\mu m^2/h^3$ range, respectively [17,18].

Interactions among mobile agents are usually modeled as a sum of pair interactions [19]. In this spirit, we factor $\vec{M}$ into

$$\vec{M}_k = \sum_{\{j\}} \frac{\vec{x}_j - \vec{x}_k}{d_{kj}}[f_1(d_{kj}) + w_j f_2(d_{kj})], \tag{2}$$

where the sum is taken over the Voronoi neighbors of particle k, and $d_{kj} = |\vec{x}_j - \vec{x}_k|$. The soft-core repulsion f_1 ensures that model cells are impenetrable. The range of repulsion is the size R_1 of the organelle-packed region around the cell nucleus. The preferential attraction response is incorporated in the f_2 term. Cells are expected to explore their surroundings with protrusions and respond when protrusions contact elongated structures. Filopodia typically extend from R_2, the cell surface ($R_1 \leq R_2$), to a maximal distance of R. Thus, $f_1(d) = 0$ for $d > R_1$ and $f_2(d) = 0$ for $d < R_2$ and $d > R$. Based on Fig. 1, we estimate $R_1 = 10$ μm, $R_2 = 30$ μm, and $R = 40$ μm. These values, however, can vary by at least a factor of 2, depending on the cell types and experimental conditions.

For the sake of simplicity, cell shape is not explicitly resolved in the model. Therefore, elongation or local anisotropy is inferred from the configuration of particles. To represent an attraction to cells within anisotropic structures, the weights w_k are constructed as

$$w_k = \frac{1}{n_k}\left|\sum_{\{j:d_{jk}<R\}} e^{2i\varphi_{jk}}\right|^2, \tag{3}$$

where the sum is taken over all n_k particles that are within a circle of radius R around particle k. The angle between

$\vec{x}_k - \vec{x}_j$ and an arbitrary reference direction is denoted by φ_{jk}. Thus, $w = 0$ for particles in an isotropic environment and $w = 1$ for particles in a highly elongated, linear configuration. Nonuniform weights result in asymmetric pair interactions, which is feasible as $\vec{M}$ represents a bias in cell activity instead of physical forces.

Equations (1)–(3) were studied by Euler integration with 0.05 h long time steps within a rectangular area of size L. Random initial and periodic boundary conditions were applied. Parameter values $\tau = 0.5$ h and $D = 100\ \mu\text{m}^2/\text{h}^3$ were chosen to represent cell motility. There is little empirical guidance on the choice of functions f_1 and f_2. We tested (i) a linear form with $R_1 = R_2 = 15\ \mu$m as $f_1(d) + f_2(d) \sim d - R_1$ and (ii) a Hertz-type repulsion $f_1(d) = -A(R_1 - d)^n$ with a zonal, distance-independent attraction $f_2(d) = B$ for $R_2 < d < R$, where the Hertz exponent n, A, and B are parameters. Irrespective of the functional forms (i) and (ii), as well as for both $n = 1$ and $n = 1.5$, a parameter regime exists in which sprout-like linear structures form during a biologically feasible time period. In Fig. 2 and subsequently, we demonstrate simulation results of model (ii) with parameters $n = 1$, $A = 160\ \text{h}^{-2}$, and $B = 130\ \mu\text{m/h}^2$. These values represent a strong response to external cues: The ratio of the directed and random velocity components is $B\tau/\sqrt{D\tau} \approx 3$. As a comparison, a similar measure for chemotactic response of endothelial cells was found larger than 1 [17].

The time development of the system was followed by the ensemble-averaged binned power spectrum $S(q) = \langle|\sum_j \exp(-2\pi i\vec{q}\cdot\vec{x}_j)|^2\rangle$, where each component of $\vec{q}$ is an integer multiple of $1/L$. The $\langle\ldots\rangle$ average is taken over configurations obtained with different noise realizations and over all scatter vectors $\vec{q}$ of length q. As Fig. 3(a) demonstrates, after an initial coarsening regime the pattern reaches a quasistationary state in which the generation of new branches balances the elimination of holes. The spectra exhibits two peaks: one at $q \approx 1/R$, reflecting the typical distance of adjacent particles, and another characterizing the pattern size at $q_* = 1/\ell_*$. In the quasistationary regime, the characteristic length $\ell_*/R \approx 10$ is independent of the system size and only weakly depends on the particle density.

The insensitivity of ℓ_* on particle density is in good agreement with the somewhat limited morphometric data available for the vasculature of quail embryos (see Fig. 3 in Ref. [3]), where $R \approx 20\ \mu$m. LaRue *et al.* characterized the vasculature with the average diameter of avascular areas M_A and the average width of vascular segments M_V. From these two quantities, we estimate the characteristic pattern size as $\ell_* \approx M_A + M_V$ and the volume fraction as $\sigma \approx 1 - M_A^2/\ell_*^2$. The five comparable data points cover volume fractions in the $0.2 \le \sigma \le 0.9$ range. The characteristic pattern size is $\ell_* = 80 \pm 15\ \mu$m with no obvious correlation between ℓ_* and σ.

As Fig. 4 demonstrates, the connectivity of the pattern depends on the particle density. We characterized the percolation transition by calculating the relative size of the largest interconnected cluster P and the volume fraction σ by treating each particle as a disk of radius R and calculating the net space coverage of the configurations. The percolation threshold is at volume fraction $\sigma \approx 0.2$: similar to the value reported in Ref. [11], and substantially smaller than 0.67, the critical volume fraction for randomly placed overlapping disks [20].

To compare our model to that of Ref. [11], we analyze the structure of the critical cluster by calculating its mean density ϱ as a function of radius r. Above the $r/R \approx 1$

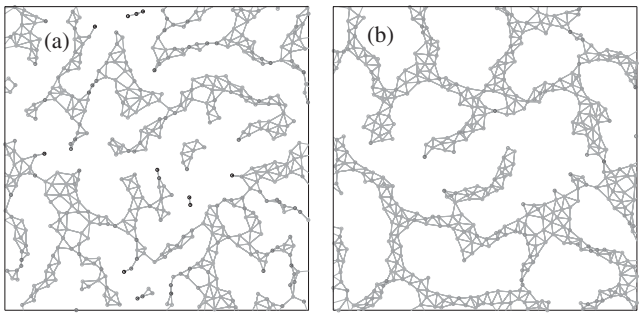

FIG. 2. Network formation in the model. Randomly placed $N = 500$ particles assemble into linear structures, detectable already within 30′ (a). At a sufficiently high particle density, a characteristic pattern size develops in five hours (b) with a combination of sprouting (branch extension) and coarsening (merger of adjacent branches). Connected dots represent Voronoi neighbor particles. Darkening gray levels indicate increasing local anisotropy. The simulation covered an area of $L = 0.7$ mm.

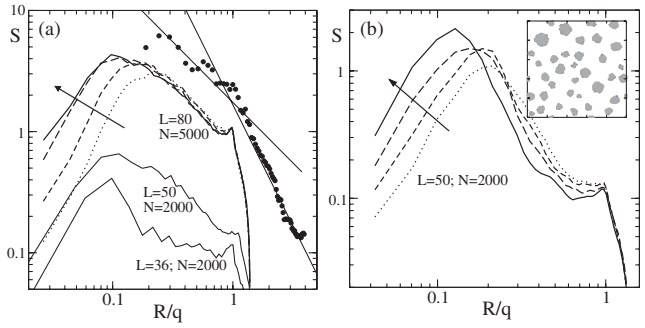

FIG. 3. Power spectrum $S(q)$ of the particle configurations, at various time points and model parameters. The dotted, dashed, and solid curves indicated by the arrows were obtained at $t = 25$, 75, 125, and 500 h, respectively. The asymmetric model (a) reaches a steady state while the symmetric model (b) continues to coarsen into droplets (inset). The shifted curves in (a) demonstrate that q_* is independent of the system size and cell density in the stationary phase. For low cell densities, the peak falls off as $1/q$, in good agreement with data obtained for Fig. 1(a) (solid symbols). The solid lines represent power-law decays with exponents -1 and -2.

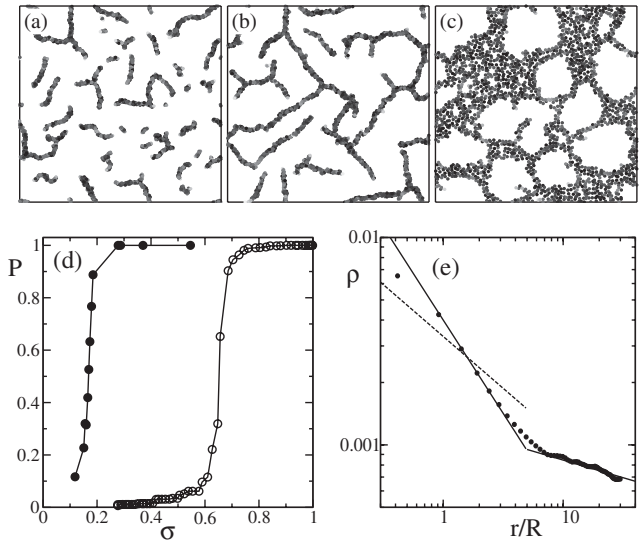

FIG. 4. Network connectivity depends on particle density. Configurations of $N = 2000$ particles are shown in the stationary phase for various values of N/L^2 particle density: (a) 0.31, (b) 0.44, and (c) 1.54. The maximal cluster size (d) shows a percolation transition at a volume fraction below 0.2 (solid symbols), much less than the critical volume fraction of randomly placed disks (open symbols). The density-density autocorrelation of the critical cluster (e) is biphasic and well approximated by $\varrho(r) \sim r^{-0.9}$ for $r < r_c$ and $\varrho(r) \sim r^{-0.2}$ for $r > r_c$ (solid lines). For comparison, the dashed line represents $\varrho(r) \sim r^{-0.5}$.

lower cutoff length, $\varrho(r)$ is well approximated by a biphasic curve: $\varrho(r) \sim r^{-0.9\pm0.05}$ for $1 < r < r_c$ and $\varrho(r) \sim r^{-0.17\pm0.1}$ for $r_c < r$. The crossover length $r_c \approx 6R$ is comparable with ℓ_*, the characteristic pattern size in the percolating regime. In agreement, for a wide range of particle densities, which includes a substantial regime above the percolation threshold, the $S(q)$ at q_* falls off to increasing q as $S(q) \sim q^{-1}$ [Fig. 3(a)]. While the obtained exponents are subject to finite size effects due to the limited scaling regime, both $\varrho(r)$ and $S(q)$ are more compatible with linear structures below $r_c \approx \ell_*$ rather than the fractal-like behavior $\varrho(r) \sim r^{-0.5}$ seen in the chemoattractant model.

In conclusion, we demonstrate that a preferential attraction to elongated cells can be sufficient to explain the abundance of networklike structures in cell cultures and that it is likely to be an important component of vasculogenic patterning. Network formation of mobile agents with spatially limited interaction range is a fundamental problem also occurring in technological fields: The establishment of a self-organized communicating network between mobile robots is one recent example [21]. We expect that a similar sprouting mechanism in a system of self-propelled agents can create adaptive networks at low volume fractions.

The authors thank E. Méhes for his help in the in vitro cell culture experiments and C. D. Little and T. Vicsek for valuable discussions. This work was supported by Grants No. 0535245N and No. 0410084Z of the American Heart Association, No. HL068855 of NIH, No. T047055 of the Hungarian Research Fund, and a grant from the G. Harold & Leila Y. Mathers Charitable Foundation.

[1] G. Forgacs and S. A. Newman, *Biological Physics of the Developing Embryo* (Cambridge University Press, Cambridge, England, 2005).
[2] W. Risau and I. Flamme, Annu. Rev. Cell Dev. Biol. **11**, 73 (1995).
[3] A. C. LaRue *et al.*, Dev. Dyn. **228**, 21 (2003).
[4] R. Vernon *et al.*, In Vitro Cell. Dev. Biol., Anim. **31**, 120 (1995).
[5] P. A. Rupp, A. Czirok, and C. D. Little, Development (Cambridge, U.K.) **131**, 2887 (2004).
[6] G. Foffi *et al.*, J. Chem. Phys. **122**, 224903 (2005).
[7] A. Czirok *et al.*, J. Microsc. **206**, 209 (2002).
[8] J. D. Murray *et al.*, in *Vascular Morphogenesis: In Vivo, In Vitro, In Mente*, edited by C. D. Little, V. Mironov, and E. H. Sage (Birkhauser, Boston, 1998), pp. 223–239.
[9] J. D. Murray, *Mathematical Biology* (Springer-Verlag, Berlin, 2003), 2nd ed.
[10] G. Serini *et al.*, EMBO J. **22**, 1771 (2003).
[11] A. Gamba *et al.*, Phys. Rev. Lett. **90**, 118101 (2003).
[12] R. M. Merks *et al.*, Dev. Biol. **289**, 44 (2006).
[13] A. E. Pelling *et al.*, Cell Motil. Cytoskeleton **63**, 141 (2006).
[14] J. Xu, Y. Tseng, and D. Wirtz, J. Biol. Chem. **275**, 35 886 (2000).
[15] D. Gray, J. Tien, and C. Chen, J. Biomed. Mater. Res., Part A **66**, 605 (2003).
[16] D. Selmeczi *et al.*, Biophys. J. **89**, 912 (2005).
[17] C. L. Stokes, D. A. Lauffenburger, and S. K. Williams, J. Cell Sci. **99**, 419 (1991).
[18] G. A. Dunn, Agents and Actions Supplements **12**, 14 (1983).
[19] D. Helbing, Rev. Mod. Phys. **73**, 1067 (2001).
[20] T. Vicsek and J. Kertész, J. Phys. A **14**, L31 (1981).
[21] I. Glauche *et al.*, Physica (Amsterdam) **325A**, 577 (2003).
[22] C. J. Drake and P. A. Fleming, Blood **95**, 1671 (2000).
[23] A. Czirók *et al.*, Phys. Rev. Lett. **81**, 3038 (1998).